JOURNAL OF PROPULSION AND POWER
Vol. 25, No. 5, September–October 2009

# Performance Modeling of a Thrust Vectoring Device for Hall Effect Thrusters

L. Garrigues,* C. Boniface,† G. J. M. Hagelaar,‡ and J. P. Boeuf§
*University of Toulouse, F-31062 Toulouse cedex 9, France*
and
O. Duchemin¶
*Société Nationale d'Étude et de Construction de Moteurs d'Aviation, 27208 Vernon, France*

DOI: 10.2514/1.39680

**The ability to control the thrust vector direction on electric propulsion devices opens new possibilities for mission optimization. The addition of an external magnetic steering system and the nonsymmetric localized injection of propellant have been proposed to deviate the ion beam of a PPS®1350 Hall effect thruster. A two-dimensional hybrid model has been used to evaluate the preliminary design. Simulated results suggest the ion beam angular distributions may be varied in the range of 10 deg by changing the current in the external steering coils. However, a magnetic topography with field lines directly connected from the outer steering pole to the anode leads to a reduction of the Hall effect thruster performance. The erosion of the walls increases drastically as a function of the magnetic lens orientation (6 mm for 1000 h of thruster operation for high coil currents in the external coils). A localized axial injection of atoms has a positive effect on the steering angle of the ion beam (a few degrees), but exhibits additional erosion of approximately 10–15%. Qualitative comparisons with experimental results confirm the simulated trends.**

## Nomenclature

| | | |
|---|---|---|
| $B_{o,x}$, $B_{o,r}$ | = | axial, radial components of the magnetic field in the centerline in the exhaust plane |
| $D$ | = | position of the injector |
| $E$ | = | ion energy |
| $E_\perp$ | = | electric field component perpendicular to the magnetic field |
| $E_{\text{th}}$ | = | sputtering energy threshold |
| $e$ | = | electron charge constant |
| $g$ | = | constant gravity on Earth |
| $I_d$, $I_i$ | = | discharge, ion current |
| $I_{\text{ion}}$ | = | ion beam divergence |
| $I_{\text{sp}}$ | = | specific impulse |
| $J_{\text{in}}$, $J_{\text{out}}$, $J_{\text{back}}$ | = | internal, external, back coil current density |
| $L$ | = | channel length |
| $\dot{m}$ | = | xenon anode mass flow |
| $m_i$ | = | ion mass |
| $m_w$ | = | mean mass of the wall material |
| $n$ | = | plasma density |
| $P$ | = | fraction of neutrals released into the channel through the ceramic wall |
| $P_w$ | = | injected power |
| $R$ | = | erosion rate |
| $T$ | = | thrust |
| $V_d$ | = | discharge voltage |
| $v$ | = | ion mean velocity |
| $Y$ | = | sputtering yield |
| $\alpha$ | = | angle between the axial axis and the ion velocity |
| $\alpha_{\dot{m}}$ | = | mean angle of the ion beam divergence |
| $\beta$ | = | magnetic field line orientation |
| $\Gamma_i$, $\Gamma_{i,\perp}$, $\Gamma_{e,\perp}$ | = | ion flux, ion, electron cross-magnetic field flux |
| $\varepsilon$ | = | electron mean energy |
| $\eta$, $\eta_u$, $\eta_c$, $\eta_E$ | = | thruster anode, propellant, current, beam energy efficiency |
| $\mu_\perp$ | = | cross-magnetic field electron mobility |
| $\rho_w$ | = | mass density of the wall material |
| $\phi$ | = | azimuthal direction |
| $\chi$ | = | number of times the current crosses the magnetic field lines |
| $\nabla_\perp$ | = | cross-magnetic field gradient |

Received 10 July 2008; revision received 4 May 2009; accepted for publication 18 June 2009. 

*Research Scientist, Centre National de la Recherche Scientifique, Laboratory Plasma et Conversion d'Energie, 118 route de Narbonne; laurent.garrigues@laplace.univ-tlse.fr.

†Currently Research Engineer, Commissariat à l'Energie Atomique, Division des Applications Militaires, F-91297 Arpajon, France; claude.boniface@cea.fr.

‡Research Scientist, Centre National de la Recherche Scientifique, Laboratory Plasma et Conversion d'Energie, 118 route de Narbonne; gerjan.hagelaar@laplace.univ-tlse.fr.

§Research Scientist, Centre National de la Recherche Scientifique, Laboratory Plasma et Conversion d'Energie, 118 route de Narbonne; jpb@laplace.univ-tlse.fr.

¶Research Engineer, Division Moteurs Spatiaux, Safran Group, Space Propulsion Division, Forêt de Vernon; olivier.duchemin@snecma.fr. Member AIAA.

## I. Introduction

HALL effect thrusters (HETs) are suitable for satellite station-keeping onboard commercial satellites and for orbit transfers of space exploration probes. Control of the thrust vector direction can be advantageous to optimize mission performance during orbital maneuvers and to overcome the displacement of the center of gravity during the mission [1]. Variation in the location of the center of gravity is mainly induced by propellant consumption and thermal deformation. A summary of thrust steering device (TSD) requirements has been detailed in [2]. Gimbal mechanisms have been proposed to change the orientation of the thruster during the HET lifetime [3]. Nevertheless, the integration of mechanical systems generates penalties (weight, complexity, integration, and test). Recent attempts to replace existing mechanisms with electrostatic or electromagnetic systems may simplify the integration and testing, and possibly decrease cost and weight as well.

In an HET, an arrangement of magnetic or electromagnetic coils leads to the establishment of a magnetic field used to confine the electrons, which allows the ionization of neutral flux by high-energy electrons. In conventional HETs, such as the PPS®1350, magnetic field lines are approximately equipotential because the electron

mobility across field lines is orders of magnitude less than the mobility along magnetic field lines. Because of the cylindrical symmetry of the system, the thrust vector deviation in the azimuthal direction due to ion beam electrostatic acceleration is negligible. To deviate the direction of thrust without mechanical displacement of the whole system, a nonzero lateral component of the force vector must be created to break the azimuthal symmetry. Several concepts have been recently identified and reviewed [4].

A promising method to produce thrust steering capability is by adding an external magnetic circuit structure to adjust the azimuthal component of the magnetic topography. As previously mentioned, the electric potential is nearly constant along the magnetic field lines, and deformation of these lines results in a deflection of the thrust vector. This system was previously tested [5] and demonstrated the capability to vary the thrust vector within $\pm 5$ deg for an SPT-100 (Russian HET of 100 mm external diameter). A three-dimensional simulation of the ion and atom dynamics, for a given electric potential based on experimental data, shows the expected azimuthal asymmetry of the ion beam for a given nonuniform azimuthal magnetic field [6].

In the standard HET configuration, the propellant is released in the discharge channel via small holes azimuthally distributed through the anode. Neutral particle collisions with the channel walls create azimuthal uniformity upstream of the ionization region. A second approach to modify the thrust vector direction is to locally inject neutrals in the discharge channel between the external pole pieces, which disturbs the azimuthal symmetry of the propellant ionization. A PPS®1350 prototype (called PPS®1350-TSD) with a modified external magnetic circuit and local propellant injection capability was assembled and tested in the Alta facility in Pisa, Italy in 2005 [7]. The investigation demonstrated a thrust vector steering angle between $\pm 8$ and $\pm 12$ deg for several combinations of the four external coil currents. Local injection of neutral propellant provided an additional 3 deg of control. The test campaign was continued in November 2007 to better quantify the effect of the steering angle on the thruster performance characteristics, behavior, and lifetime [8].

In this paper, the effects of the additional external magnetic circuit structure and the local injection of propellant are compared with numerical results from a two-dimensional axisymmetric hybrid model [9,10]. This study follows one of the concepts proposed in [4], where the local injection of neutral atoms is considered as a secondary system to increase the steering angle, but it is not considered as the only technique to deviate the thrust vector direction. The main objectives of this study are to evaluate the modification of the external magnetic field and neutral flow injection on 1) the thruster performance, 2) the ion beam angle deviation, and 3) the erosion of the channel walls. Although the two-dimensional model differs from the three-dimensional configuration required, the simulated results are a useful resource to examine the preliminary design based on simple magnetic considerations [2]. In Sec. II, the modifications of the PPS®1350 geometry and magnetic field configurations are studied. The hybrid model is briefly described in Sec. III. The two-dimensional simulations in Sec. IV illustrate the effect of the modified magnetic field topography and the local injection of neutral flow on the thruster behavior, assuming that the anomalous electron cross-magnetic field remains unchanged. In Sec. V, experimental results are compared with the model results and limitations of the approach are discussed. The two-dimensional solutions have been used as starting conditions in a three-dimensional plume model to characterize the thrust vector that can be compared with previous experimental test campaigns [7,8]. The main conclusions are summarized in Sec. VI.

## II. PPS®1350-TSD Description

This section describes the modified PPS®1350-TSD thruster geometry and reviews the different magnetic field topologies obtained by varying the coil currents in the external steering structure.

### A. PPS®1350-TSD Geometry

The PPS®1350-TSD has a standard annular geometry channel consisting of two coaxial ceramic cylinders, with an anode at one end and a cathode on the outside at the other end. The neutral propellant is uniformly injected inside the channel through an arrangement of small apertures positioned around the anode plane. The main characteristics are summarized in Table 1.

**Table 1 Properties of the PPS®1350 thruster studied in this work**

| Property | PPS®1350 |
|---|---|
| Outer diameter, mm | 100 |
| Nominal mass flow, mg/s | 5.2 |
| Nominal applied voltage, V | 350 |

The magnetic field structure of the channel zone of the PPS®1350-TSD consists of (see Fig. 1a) [2] 1) a magnetic circuit with pole pieces, cores, and magnetic screens; 2) an internal coil with a current density $J_{\text{in}}$; 3) four external coils with a current density equal to $\pm J_{\text{out}}$; and 4) a back coil with a current density $J_{\text{back}}$.

The original outer pole piece of the PPS®1350 has been slightly modified to support the additional magnetic structure outside the channel made of 1) a magnetic circuit with a cylindrical core, and 2) four external steering coils placed on the four corners of the front plate with varying current density.

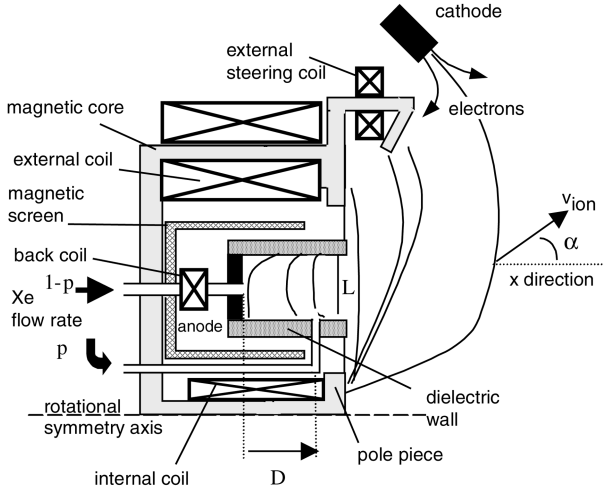


a)

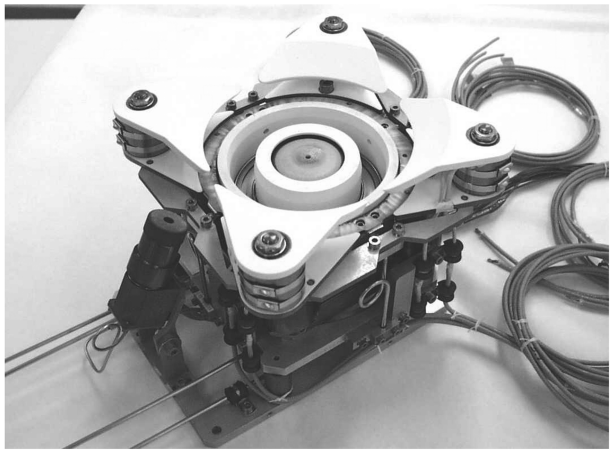

b)

**Fig. 1 PPS®1350-TSD a) scheme used for thrust steering, where *L* is the channel length, *P* is the fraction of xenon propellant injected through the local nozzles (1-*P* will be the anode mass flow injected), and *D* is the axial position where the xenon is injected through the ceramic walls, and b) photo [7].**

The magnetic steering coils of the external structure are powered by separate power supplies. For simplicity, the current densities in internal, external, and back coils remain the same throughout this study. Modeling the four external steering coils with a 2-D simulation introduces several difficulties, which were resolved following the method presented in [11,12]. The four steering coils were substituted with two coaxial coils with currents equal in magnitude but opposite in direction. The two coils are separated by a ferromagnetic cylinder, the mean radius of the magnetic structure being positioned at the same radius passing through the center of the four original coils. The section of the ferromagnetic element is deduced from the real sections of the four external coils. The same method has been successfully used in the context of the PPS®1350 to model the 3-D arrangement of similar magnetic field structure [11,12]. In this study, different external steering coil currents were evaluated to deviate the thrust vector direction. In the reference case, designated case 1, the external steering coil is not powered. Cases 2 and 4 examine the effect of the external steering coil current density equal to 0.6 and 1.1 $J_{\text{out}}$, respectively. Cases 3 and 5 consider the same current density magnitudes in the opposite direction as cases 2 and 4, where case 3 is $-0.6\ J_{\text{out}}$ and case 5 is $-1.1\ J_{\text{out}}$. The external steering coil conditions are summarized in Table 2.

The effect of asymmetric propellant injection on the steering effect was investigated by locally injecting neutral atoms downstream of the anode through the ceramic walls. In this study, the total mass flow rate to the thruster is conserved to maintain approximately the same discharge current and total power. The local injection is therefore not a supplementary injection of neutrals. The fraction of xenon propellant injected through the localized nozzles is denoted $P$, and (1-$P$) is the mass flow fraction supplied to the anode. The injected propellant fraction $P$ is varied from 0 to 0.5. The axial location of injected neutrals is shown as $D$ in Fig. 1a. A photo of the assembled PPS®1350-TSD is displayed in Fig. 1b.

### B. Magnetic Field Configurations

The magnetic field topographies of cases 1–5 are shown in Fig. 2. Recall that, in case 1, the external steering coils are not powered. The orientation of the magnetic field lines depends on the magnitude and the sign of the coil currents. More precisely, the magnetic field lines are directed toward the thruster centerline axis of symmetry (cases 2 and 4) when the current flowing through the steering coils is in the same direction as in the external coils. The orientation of the magnetic field is directed in the opposite direction when we reverse the current direction in the external steering coils (cases 3 and 5).

We have chosen to quantify the magnetic field orientation using the $\beta$ angle written as $\beta = -\tan^{-1}[B_{o,x}/B_{o,r}]$, where $B_{o,x}$ and $B_{o,r}$ are, respectively, the axial and radial components of the magnetic field in the middle of the channel at the exhaust plane. That is an easy way to examine the effect of external coil currents on the magnetic field lines orientation. Table 2 summarizes the values of the $\beta$ angle for the five cases studied. The magnitude of the inclination depends on the magnitude of the coil currents in the additional steering configuration. The analysis of the $\beta$ angle is not sufficient to completely analyze the influence of the coil currents on the magnetic field topology. In Fig. 2, we have also plotted the radial magnetic field profile along the thruster centerline and walls. As expected, the magnitude of the magnetic field in the region outside the thruster channel increases as the current density of the external steering coil increases, while the magnitude of the magnetic field inside the channel remains nearly constant. However, if we observe the inner profile, we note a small variation of the position of the zero-magnetic field.

**Table 2 Five magnetic configurations tested for thrust steering in this paper**

| Case no. | Coil current densities | $\beta$ angle, deg |
|---|---|---|
| 1 | 0 | −9 |
| 2 | $\pm 0.6\ J_{\text{out}}$ | −20 |
| 3 | $\pm 0.6\ J_{\text{out}}$ | +1 |
| 4 | $\pm 1.1\ J_{\text{out}}$ | −28 |
| 5 | $\pm 1.1\ J_{\text{out}}$ | 13 |

The consequence of the TSD pole pieces extends inside the thruster channel. In case 2 and case 4, a large axial component of the magnetic field is observed at the exhaust plane. Moreover, some magnetic field lines connect the external steering pole to the anode plane (as indicated in gray in Fig. 2). This means that one electron trapped around the magnetic field line that intercepts the anode is rapidly collected by the latter. The consequences of this effect on discharge properties will be discussed later. We come back to the real 3-D magnetic configuration effect on the steering angle in Sec. V.

## III. Overview of the Two-Dimensional Axisymmetric Hybrid Model

The two-dimensional axisymmetric hybrid model is described in Sec. III.A. Analysis of ion beam parameter calculations, such as performance and ion beam distribution, are outlined in Sec. III.B, and the methodology used to calculate wall erosion due to energetic ion collisions is explained in Sec. III.C.

### A. Review of the Hybrid Model

Details of the two-dimensional hybrid model have been described in previous publications [9,11]. The computational domain in the axial and radial directions accounts for the discharge channel and the near-field region extending to the cathode. The computational domain ends at the magnetic field line intercepting the cathode. The TSD magnetic structure has been incorporated into magnetic field topography simulations, but the structure remains outside the computational domain. The electrons are treated using quasi-one-dimensional fluid equations, and the heavy species are treated using macroparticles, as in the well-known particle-in-cell (PIC) approach. Neutral atoms are injected through the anode plane, and localized injection through the ceramic walls is approximated by a point source releasing propellant perpendicular to the channel wall [13]. The model assumes quasi neutrality. The plasma density is deduced from ion PIC simulations, where only single charged ions are modeled in this study. The electric field is inferred from the electron fluid transport.

Electron diffusion along the magnetic field lines is several orders of magnitude higher than the diffusion across the magnetic field lines. As a result, electrons are assumed to follow a Boltzmann distribution along the magnetic field lines and a drift-diffusion equation is used to calculate the electron flux in the direction perpendicular to the magnetic field lines:

$$\Gamma_{e,\perp} = -\mu_\perp E_\perp n - \frac{2}{3e}\mu_\perp \nabla_\perp (n\varepsilon) \tag{1}$$

where $\mu_\perp$ is the cross-field electron mobility, $n$ is the plasma density, $\varepsilon$ is the electron mean energy, $e$ is the elementary charge, and $\nabla_\perp$ represents the cross-field gradient. The electric field component $E_\perp$ perpendicular to the magnetic field is now obtained by substituting this equation in the current conservation equation

$$e \iint \Gamma_{e,\perp}\, \mathrm{d}s = e \iint \Gamma_{i,\perp}\, \mathrm{d}s - \frac{\chi}{e} I_d \tag{2}$$

where $\Gamma_{i,\perp}$ is the cross-field ion flux and the integrals are taken along magnetic field lines (surfaces). The factor $\chi$ represents the number of times the current crosses the magnetic field lines. The coefficient $\chi = 1$ for the magnetic field lines between the anode and the cathode, and $\chi = 0$ for the magnetic field lines that close themselves on the outer and inner walls. The discharge current $I_d$ is calculated self-consistently such that a specified voltage drop results between the electrodes. It is assumed that no net current escapes to the insulating channel walls.

The ionization rate is calculated with the help of an energy equation assuming a Maxwellian distribution function. This energy

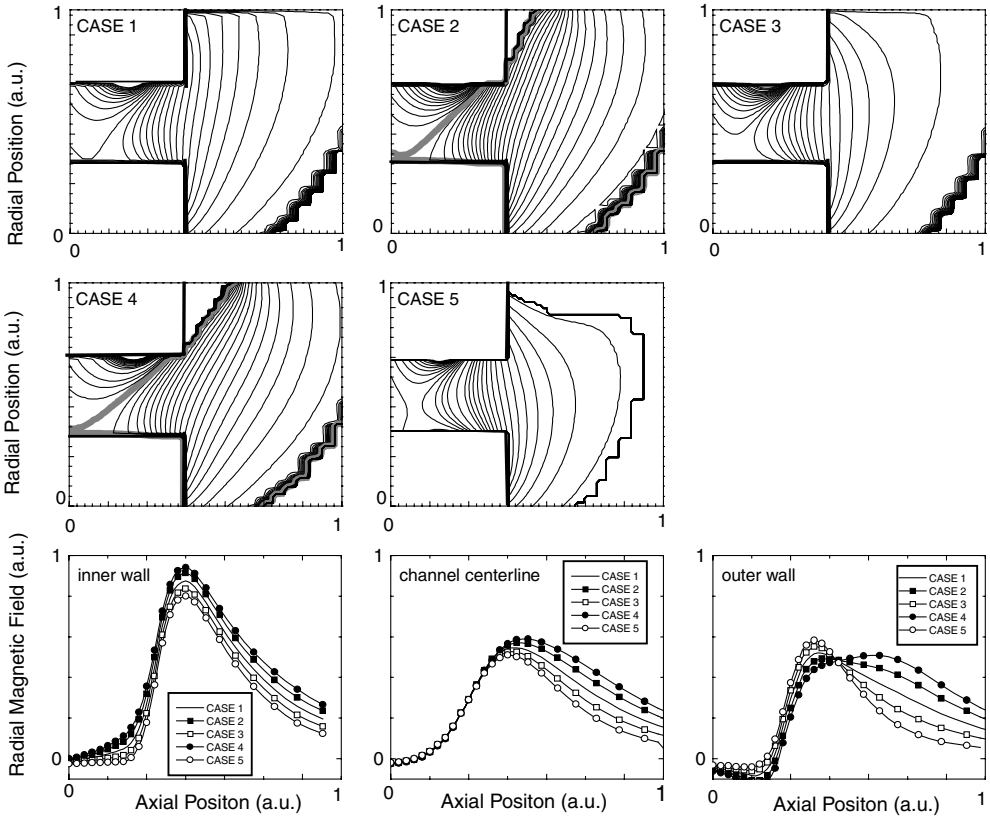


**Fig. 2 PPS®1350-TSD magnetic field lines calculated with Finite Element Method Magnetics software for different sets of coil currents in the external structure. Axial variations of the calculated radial magnetic field strength along the channel centerline and inner and outer walls for different magnetic configurations.**

equation includes Joule heating and electron energy losses due to electron–atom inelastic collisions and electron–wall interactions.

The main challenge in the fluid model of the electron transport is to properly calculate the mobility that accounts for electron diffusion across the magnetic field lines, especially in the region of high magnetic field magnitude and low neutral densities. Various theories have been proposed, such as electron–wall interactions or Bohm-type diffusion [14] to explain the cross-field electron diffusion. In this paper, parametric coefficients are used to quantify this anomalous electron diffusion. This paper is based on the study of a modified PPS®1350 thruster. Because the magnetic field profiles (and magnetic field magnitude) are rather close to ones of the conventional HET, the anomalous coefficients are the same as the ones proposed by Bareilles et al. [15]. We must emphasize here that small variations around the coefficients selected for this study do not change the conclusions. We have characterized this phenomenon and adopted the simplest (but not perfect) approach by holding the coefficient to a constant value for all the studied cases.

### B. Ion Beam Parameters

To characterize the (time-averaged) HET performance, three parameters are evaluated. The first parameter is the thrust $T$, defined as the resultant force opposite to the acceleration of the ions (including the minor force exerted by ions impinging on the channel walls)

$$T = \left(\frac{m_i I_i}{e}\right)\langle v\cos\theta\rangle \tag{3}$$

where $m_i$ is the ion mass, $I_i$ is the current carried by the ions leaving the thruster, $v$ is the mean velocity of the ion velocity distribution function, $\theta$ is the angle this makes with respect to the thruster axis, and $e$ is the elementary charge. The bracket indicates an average over the ion current distribution (the term $\langle v\cos\theta\rangle$ is thus the axial mean velocity of the ions). We totally neglect the influence of the neutral flux on the thrust.

The second parameter is the specific impulse $I_{\rm sp}$ (impulse per unit weight) which is proportional to $T$ and inversely proportional to the xenon mass flow rate $\dot{m}$:

$$I_{\rm sp} = \frac{T}{\dot{m}g} \tag{4}$$

$g$ is the gravity constant on the Earth ($g = 9.81\ \mathrm{m\cdot s^{-2}}$). If the gas is totally ionized, the specific impulse is equal to the ion mean velocity in the axial direction divided by the gravity constant $g$.

The final parameter studied is the thruster anode efficiency $\eta$, which compares the kinetic output power to the injected power ($P_w = I_d V_d$, where $I_d$ is the discharge current and $V_d$ is the applied voltage):

$$\eta = \frac{T^2}{2\dot{m}I_d V_d} \tag{5}$$

Note that the supplementary injection of xenon into the cathode is not included in the thruster anode efficiency calculation. If all ions are assumed singly charged, thruster efficiency can be written as the product of different terms as proposed by [16], where each term contributes to the total loss of energy for the thruster:

$$\eta = \left(\frac{m_i I_i}{e\dot{m}}\right)\left(\frac{I_i}{I_d}\right)\left(\frac{m_i\langle v\cos\theta\rangle^2}{2eV_d}\right) \equiv \eta_u\eta_c\eta_E \tag{6}$$

The first factor $\eta_u$, known as the propellant efficiency, characterizes the proportion of propellant being ionized. The factor $\eta_c$, called the current efficiency, characterizes the loss of electron current to the anode. The beam energy efficiency $\eta_E$ is the ratio of the mean energy of the ion beam leaving the thruster to the maximum energy the ions can obtain. The beam efficiency is referred to as the acceleration efficiency in [16] (also called voltage utilization efficiency). We

include in the beam energy efficiency the losses due to the spread of the ion velocity distribution function and due to the divergence of the beam (which are often separated in the HETs literature [16]).

The ion beam divergence $I_{\text{ion}}$ was characterized by integrating all the ions leaving the computational domain as in [15]. The deviation of the ion velocity from the axial direction is called $\alpha$ (see Fig. 1). The mean angle of the ion beam divergence is defined as follows:

$$\alpha_m = \frac{\int \alpha I_{\text{ion}}(\alpha)\, \mathrm{d}\alpha}{\int I_{\text{ion}}(\alpha)\, \mathrm{d}\alpha} \tag{7}$$

### C. Sputtering Model

The erosion model, which accounts for sputtering due to the influence of high energetic ions on the ceramic walls, has been previously described [10,17]. The erosion rate $R$ (eroded thickness per unit time) is proportional to the ion flux impacting the walls $\Gamma_i$ and to the sputtering yield $Y$ (number of eroded atoms per incident ions for an incident energy $E$ and for an incidence angle of $\phi$):

$$R = \frac{\Gamma_i m_w}{\rho_w} \langle Y(E, \phi) \rangle \tag{8}$$

where $m_w$ and $\rho_w$ are the mean mass and the mass density of the wall material, respectively. The triangular brackets indicate an average over the incident ion flux distribution. The sheath potential drop is added to the ion energy impinging the ceramic walls [18]. It is difficult to ascertain information about the influence of the ion energy on the sputtering yield over a large energy range, especially for incident ion energy below 100 eV. An analytical formula has been derived from the work of [19] to account for the energy influence on the sputtering processes. In this approach, the uncertainty of the erosion calculations is linked to an assumed sputtering energy threshold $E_{\text{th}}$. This analytical model limits the quantitative calculations of the ceramic erosion, however, it provides qualitative information about the influence of the discharge parameters on thruster wall erosion. Recent results show that an energy threshold $E_{\text{th}}$, varying in the range of tens of electron volts, provides reasonable magnitude of the erosion rate for a conventional HET [18]. In this study, the $E_{\text{th}}$ parameter is accordingly fixed to 50 eV. This value has been adopted in another recent study to predict the transient evolution of the ceramic wall erosion up to 4300 h for an HET with a longer channel [17]. The sputtering yield angular dependence is deduced from measurements [20].

## IV. Two-Dimensional Calculations of Thruster Properties

The goal of the two-dimensional model is to examine the qualitative effect of the magnetic TSD pole pieces and neutral atom injection on the possible deviation of the ion beam and the consequence of increased erosion of the ceramic walls. The effects of the magnetic field configuration without additional propellant injection through the ceramics is analyzed. Specifically, the effects on thruster performance, on ion beam divergence, and on the erosion of the thruster walls are studied in Sec. IV.A. The combined effects of the TSD pole pieces with localized atom injection through the ceramic walls is examined in Sec. IV.B. Throughout this study, the applied voltage is fixed to 350 V and the total xenon mass flow released in the channel is 5.2 mg/s.

### A. Influence of the Magnetic Field Configuration

The time-averaged thruster performance is calculated for the configuration where the xenon flow is not injected through the localized nozzles, and the parameter $P$ is therefore fixed to zero. Results are summarized in Table 3. A lower ion current is clearly seen in cases 2 and 4. The propellant efficiency $\eta_u$ is significantly reduced to less than 0.85. The spatial distribution of the ionization source term (number of electron–ion pairs created per unit time and per unit volume) and the profile of the electric potential are displayed in Fig. 3. The spatial distribution of the electric potential is related to the magnetic field profile, as expected. In case 4 (and in case 2 not shown here), the ion production is weaker near the outer wall and the ionization zone is concentrated near the inner wall. Near the inner wall region, the magnetic field lines are directly connected from the outer steering pole to the anode, collecting the electrons. The residence time of the electrons is then too low to efficiently ionize neutral flux, leading to reduced thrust and specific impulse. This result indicates that such a magnetic field topography modified for steering would decrease performance. The thruster efficiency $\eta$ is lower than 0.45 for cases 2 and 4, and $\eta$ is greater than or equal to 0.5 in cases 3 and 5. We can attribute the reduction of thruster efficiency for cases 2 and 4 to the low propellant efficiency. Finally, the beam energy efficiency $\eta_E$ is low in cases 2 and 4, which can be explained by a larger divergence of the ion beam. We have to point out here that part of the reduction in the thruster efficiency in cases 2 and 4 must be attributed to the definition of the thrust [we have chosen to calculate the force in the axial direction; see Eq. (3)]. If we consider a given steering angle, the overall performance loss is obviously less than indicated in Table 3.

The ion beam divergence and the mean angle of the ion beam divergence $\alpha_m$ from Fig. 4 is reported in Table 3. The shape of the ion beam divergence is totally different according to the orientation of the coil currents. In the case of positive external current (cases 2 and 4), the maximum of the ion distribution is clearly shifted. Case 1, with no current through the steering coils, exhibits a deviation angle of 12.6 deg. When the external steering coils are powered with a low current (60% of the outer coil current), the mean angle reaches 17 deg in case 2 and 12 deg in case 3. To achieve a higher thruster steering angle, increasing the current in the external steering coil to a value comparable to the outer coil current deviates the mean beam angle 21 and 17 deg for case 4 and case 5, respectively.

One important consequence of the ion beam deviation is the possible erosion of the ceramic walls due to ion impact. This effect is quantified by calculating the erosion rate due to ion bombardment. A refined prediction of the eroded profiles as a function of time is difficult, regardless of the assumptions related to the calculations of the erosion rate itself. The erosion rate simply decreases with time because the channel profile is eroded, and no attempt is made to predict the history of the erosion profile. Nevertheless, the initial calculated erosion rate is an adequate indication of the thruster lifetime. Figure 5 illustrates the calculated erosion of the inner and the outer walls in the axial region between $0.75 \times L$ and $L$ ($L$ being the channel length). The influence of the direction of the ion beam on the channel erosion is clearly demonstrated. The outer wall experiences a higher erosion rate for negative external coil current and the inner wall is eroded for a positive steering coil current. The thickness of the material eroded is related to the magnitude of the coil currents of the external structure. The erosion of the walls is asymmetric according to the orientation of the ion beam. Case 1 displays a relative low erosion rate (negligible for the outer ceramic, and only 2 mm for 1000 h for the inner wall). A high ion beam deviation angle (case 4) leads to an estimated inner wall erosion of 6 mm for 1000 h of thruster operation in the exhaust plane. A low ion beam angle deviation (case 2) reduces the magnitude of the erosion (4 mm in case 2).

**Table 3 Time-averaged calculated performance and mean angle of the ion beam distribution of the PPS®1350-TSD for steering obtained with the two-dimensional hybrid model**

| Case no. | 1 | 2 | 3 | 4 | 5 |
|---|---|---|---|---|---|
| $I_d$, A | 4.3 | 3.75 | 4.61 | 3.21 | 4.9 |
| $I_i$, A | 3.70 | 3.05 | 3.50 | 2.70 | 3.5 |
| $T$, mN | 88 | 77 | 92 | 65 | 91 |
| $I_{\text{sp}}$, s | 1737 | 1510 | 1800 | 1270 | 1783 |
| $\eta$, thruster anode eff. | 0.49 | 0.43 | 0.50 | 0.36 | 0.46 |
| $\eta_u$, propellant utilization | 0.88 | 0.80 | 0.91 | 0.70 | 0.92 |
| $\eta_c$, current efficiency | 0.78 | 0.81 | 0.76 | 0.83 | 0.72 |
| $\eta_E$, beam energy | 0.72 | 0.67 | 0.72 | 0.61 | 0.69 |
| mean angle $\alpha_m$, deg | 12.6 | 17.3 | 12.1 | 21 | 17 |

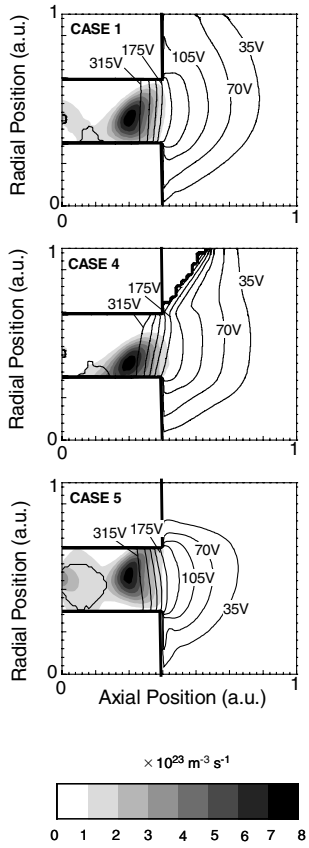


**Fig. 3 Time-averaged spatial profile of the electric potential (contours) and ionization source term (grayscale) for case 1, case 4, and case 5. The 10 contours are equally spaced from 0 to 350 V, and the eight grayscale intervals correspond to $10^{23}$ $m^{-3}$ $s^{-1}$ each (from 0 to $8 \times 10^{23}$ $m^{-3}$ $s^{-1}$).**

### B. Effect of Magnetic Field Configuration with a Supplementary Injection of Neutrals

Numerical simulations of local xenon injection through the ceramic nozzle were performed using two free parameters, including the position of the injector (called $D$; the reference $D = 0$ is taken on the anode plane) and the fraction of neutrals $P$ released into the channel through the ceramic wall (1-$P$ being the fraction of neutral flux injected through the anode plane).

Local injection of xenon through the inner ceramic is only considered for cases 3 and 5, and through the outer ceramic for cases 2 and 4. This decision is based on the desired beam angle deflection. To reduce the range of variations of $D$ and $P$, the fraction of propellant injected through the anode injector $P$ is varied from 0 to 0.5. Auxiliary injection of neutrals between the anode plane and the ionization region (between 0 and $0.5 \times L$) are neglected, because

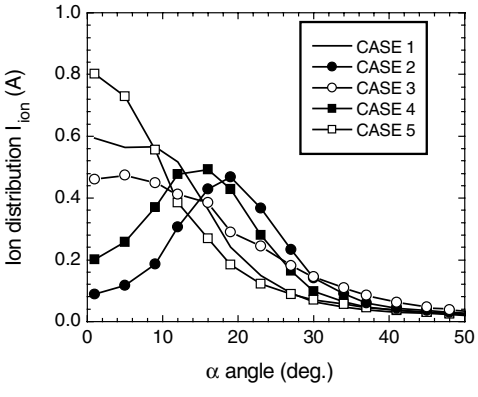


**Fig. 4 Ion distribution function as a function of the angle.**

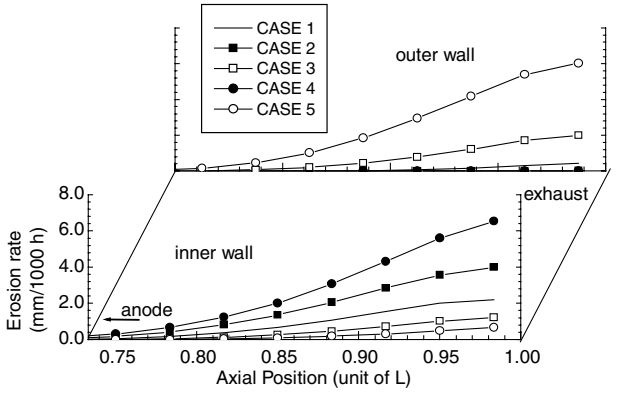


**Fig. 5 Calculated erosion rate for inner and outer walls without a supplementary injection of neutral atoms.**

neutral flux injected near the anode will collide with the walls before entering the ionization zone. The neutral density will then be homogenized before being ionized, and the supplementary effect of neutral injection through the ceramic walls on the angular deviation will be negligible. Injection of atoms in the region downstream of the ionization zone leads to an important un-ionized flux of atoms and a low performance of the engine. Therefore, the effect of the auxiliary injection of neutrals is studied for $D$ varying from $0.55 \times L$ to $0.9 \times L$. Thruster anode efficiency $\eta$ is not significantly affected by a local gas injection within the selected regions.

Results displayed in Fig. 6 show that the thruster efficiency of case 5 is approximately unchanged, except when $P$ is in the range of 0.3–0.5 and for $D$ between $0.73 \times L$ and $0.83 \times L$. In this region, the propellant efficiency $\eta_u$ is ~0.7, compared to 0.9 for case 5 without neutral injection through the walls. The influence of $D$ and $P$ on the ion beam angle deviation is shown in Fig. 7 for case 5, where the angle $\alpha_m$ is displayed for a given percentage of neutral flow injected through the inner ceramic. When equal neutral flow is delivered through the anode plane and through the auxiliary injection nozzles ($P = 0.5$) for a position of the injector $D$ between $0.73 \times L$ and $0.83 \times L$, the angle of deviation of the ion beam reaches 22 deg, which is an increase of 5 deg compared with the $P$ factor equal to zero. However, thruster efficiency is reduced in these conditions by approximately 10%, as seen in Fig. 6. A $P$ factor of 0.1 leads to only a 1 or 2 deg supplementary beam angle deviation. Typically, the same trends are seen in the low and high coil current configurations.

In Fig. 8, the erosion rate of the outer ceramic for case 5 is illustrated as a function of the fraction of neutrals injected $P$ and the

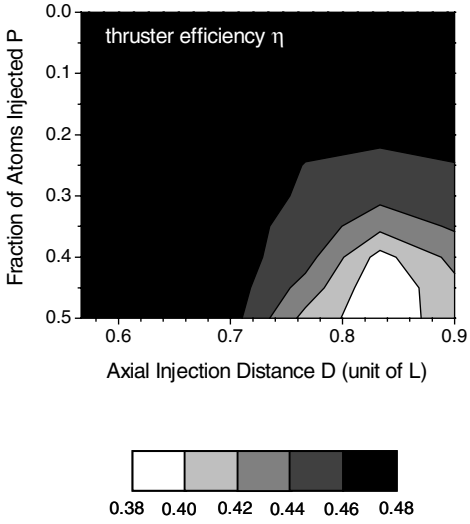


**Fig. 6 Thruster anode efficiency $\eta$ as a function of $D$ and $P$ for case 5. The five levels are equally spaced from 0.38 to 0.48.**

position of the injection $D$. Neutral flow is injected through the inner ceramic. The white line corresponds to an erosion rate equal to 6 mm, which corresponds to an erosion rate without a supplementary injection of neutral atoms in case 5. The erosion rate reaches 7 mm/1000 h for a large fraction $P$ and a position $D$ at $0.65 \times L$. When $D$ increases, the erosion rate also decreases down to the same magnitude as the configuration without any additional injection. The erosion rate of the inner ceramic in case 5 (not shown here) is still negligible.

## V. Three-Dimensional Configurations

This section describes experimental results of the modified thruster configuration (Sec. V.A) and details the approach used to calculate the steering angle in three dimensions (Sec. V.B). Comparisons between calculations and experimental results are evaluated (Sec. V.C). A short discussion follows on possible explanations of the discrepancies and differences between 2-D simulations and 3-D experimental data (Sec. V.D).

### A. Description of the Configurations Tested to Steer the Thrust Vector

A prototype thruster, called PPS®1350-TSD, has been designed and tested to evaluate two methods of steering the thrust vector direction, as sketched in Fig. 9 [7]. The first configuration in Fig. 9a, designated L1, consists of powering the four external steering coils. Two adjacent coils have the same current direction, and the two opposing coils are supplied with equal current in the opposite direction. The beam deflection is along the $z$ direction. In the second configuration reported in Fig. 9b, designated L2, two opposing coils are powered with equal currents in opposite directions, and the remaining two are unpowered. The steering angle will be in the plane passing through the two powered coils at 45 deg from the steering angle of L1. The sites of additional local neutral injection are also shown in Fig. 9. Either one or two nozzles are used to deflect the beam angle, and the xenon injection is located between two adjacent coils for technical reasons.

In practice, voltage and current probes are introduced to measure the discharge parameters. Nevertheless, the beam current density profiles cannot be used as data to derive the thrust vector direction for numerous reasons, explained in [8]. The axial and horizontal transverse components of the thrust vectors were measured using a two-axis thrust stand, based on a double direct pendulum configuration. The arms of the pendulum consist of a thin plate (flexure) which is bent by the thrust from the engine (see Fig. 10). Each flexure is equipped with two optical strain gauges that measure the bending strain. A calibration coefficient relates the bending to the applied force. The bending strains for each axis are averaged over the two flexures and the relative calibration coefficient is used. The calibration is carried out independently for each axis before and after the test campaign. The force steps are controlled by moving the load cell with a precision micrometer. More details on the experimental apparatus can be found in [7,8].

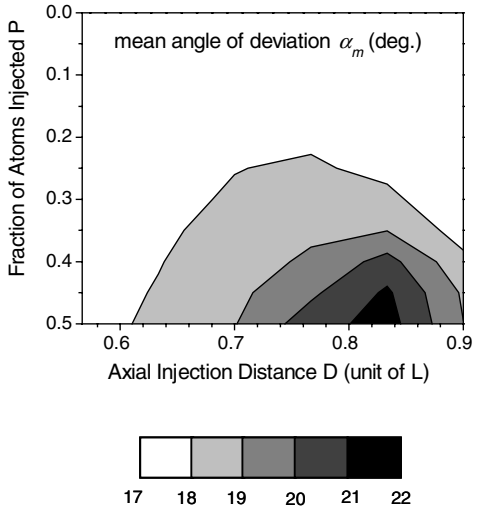


**Fig. 7 Mean angle of beam deviation $\alpha_m$ as a function of $D$ and $P$ for case 5. The five levels are equally spaced from 17 to 22 deg.**

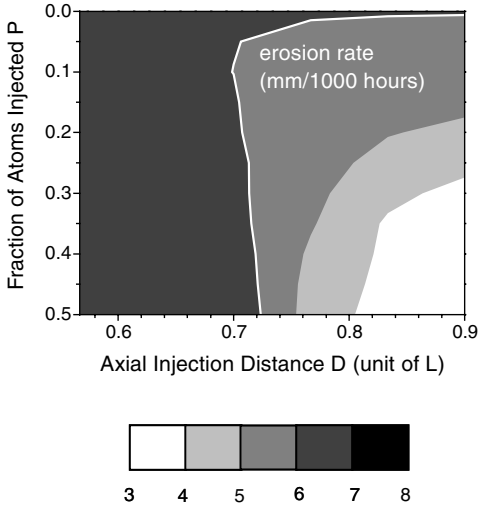


**Fig. 8 Calculated erosion rate for the outer ceramic for case 5 with a supplementary injection of neutral atoms.**

### B. Three-Dimensional Plume Model Approach

Because a complete three-dimensional HET model starting from the anode plane and finishing beyond the cathode does not yet exist,

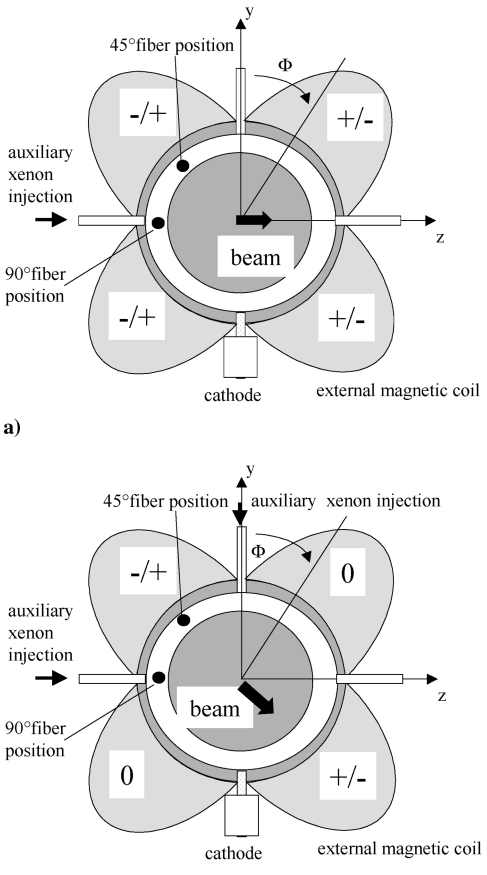


**Fig. 9 Front view of scenarios of the ion beam deviation studied in [7]. The optical fiber positions are also presented.**

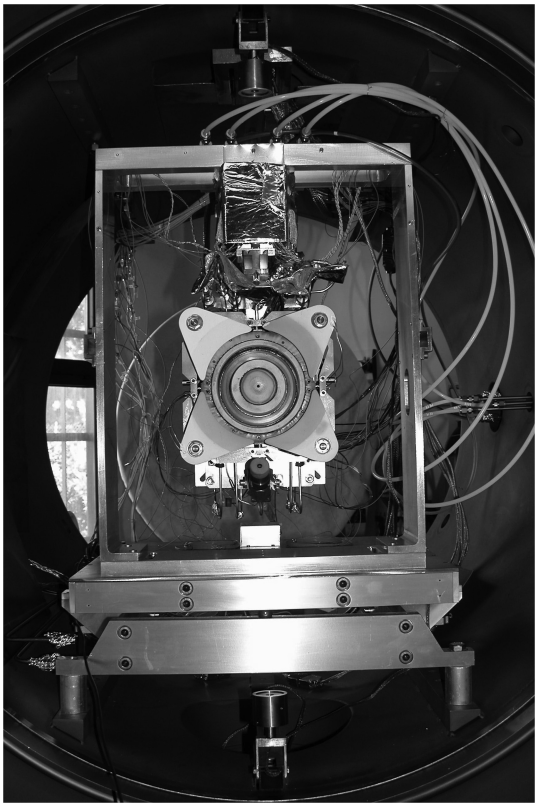

**Fig. 10 Photo of the PPS®1350-TSD mounted on the two-axis thrust stand with calibration equipment [7].**

the three-dimensional problem has been approached by the following method. The output from the two-dimensional model (ion and neutral distribution functions, electric potential) are taken in the exhaust plane for a given corresponding azimuthal angle $\Phi$ (see Fig. 9 for notations) and for one specific case previously studied with the two-dimensional model. The "real" three-dimensional initial conditions must be assessed from a superposition of two separate cases (case 2 and case 3 for low steering angle, case 4 and case 5 for high steering angle) for configuration L1, or three cases (case 1, case 2, and case 3 for low steering angle; case 1, case 4, and case 5 for high steering angle) for configuration L2. The ion and neutral distribution functions, as a function of azimuthal angle $\Phi$, are obtained using linear interpolation by imposing them at two or three corresponding initial $\Phi$ angles. These distribution functions serve as initial conditions for complete three-dimensional calculations of the plume [2], where the densities of heavy species are calculated from the integration of the movement of a large number of ions and neutrals, the electron density is calculated assuming a Boltzmann equilibrium, and the electric field is deduced from a Poisson equation [21]. The main assumptions of this approach are that the interactions between two adjacent coils can be neglected, and that the local injection of atoms is located in the same plane as the external magnetic structure.

### C. Comparisons Between Experiments and Calculations

The ion beam angle was calculated with a three-dimensional plume model and compared to experimental results for low and high external steering coil current conditions with no local gas injection. Experimental results give a steering angle of 4 and 8 deg for L2, and 8 and 12.5 deg for L1, when the external coil currents in the external structure increase from 0.6 to 1.1 times the current of the outer coil. Calculated steering angles for the same conditions result in 3.5 and 7.5 deg for L2, and 5 and 11 deg for L1 [7], in agreement with the measured values. The thrust steering angle is lower in the L2 configuration because only two steering coils are powered. Measurements on the PPS®1350-TSD have also been performed using an auxiliary xenon feed system to release a small, precise amount of neutral atoms through nozzles (the fraction $P$ varies between 0 and 0.1 in the experimental conditions). Roughly, measurements of the thrust steering angle have demonstrated additional steering capability of a few degrees, comparable to simulated results. The measured experimental total thrust magnitude ranges from 82–90 mN when the two configurations L1 and L2 (with and without additional neutral flow) are tested. The total thrust magnitude computed for the different configurations using the three-dimensional plume model varied between 83 and 92 mN [2].

Measurements of discharge current show a large increase (up to 20%), with a corresponding reduction of the thruster efficiency ($\eta = 0.3$), in the L1 configuration when the four coils are powered. Computed efficiency with the plume model does not exhibit such a reduction in the thruster efficiency in the L1 configuration. Nevertheless, the two-dimensional hybrid model indicates that a low discharge current does not always correlate to a large anode efficiency. In Table 3, cases 2 and 4 exhibit a low discharge current accompanied with a low ion current. The reduction in the thruster efficiency may be due to the magnetic field configuration and the lines which connect the cathode directly to the anode, as previously mentioned in Sec. IV.A.

The erosion of the thruster walls has been estimated through optical emission spectroscopy [22], with the optical fiber positioned at 45 and 90 deg with respect to the $z$ axis, as shown in Fig. 9. The ion beam was steered for several operating conditions with and without a localized injection of neutral atoms, and the erosion rate has been reconstructed. Note that no calibration can be made, and the signal collected only gives relative values of the erosion rate. When the optical fiber is positioned at 90 deg, a local erosion factor up to 1.8 was measured for the case of no localized propellant injection (the reference factor equal to 1 is chosen for zero current in the four external coils). This factor increases to 5.5 when a local propellant injection is added ($P = 0.05$). Three-dimensional reconstruction of the eroded profile has not been investigated. In the two-dimensional calculations, the erosion rate does not demonstrate the same tendency for such a low fraction of neutral atoms injected through an additional nozzle (see Fig. 8).

### D. Origin of the Discrepancies Between Experiments and Calculations

The origin of the discrepancies between the experimental and calculated results can be attributed to three-dimensional effects (interactions between adjacent coils, localized atom injection) that cannot be taken into account in a two-dimensional axisymmetric model. The influence of two adjacent TSD pole pieces with opposite polarities has been recently studied in detail through three-dimensional modeling of the magnetic circuit [8]. A distortion in the azimuthal magnetic field has been demonstrated. Variation in the azimuthal magnetic field leads to a change in the axial electron mobility (and consequently in the electron component) that can be responsible for the observed trends in the experimental results in the L1 configuration. The effect of the air gap between two TSD pole pieces on the erosion profile has been also noticed. The injection of neutral atoms through the ceramic walls is assumed to be azimuthally symmetric. A localized injection of neutrals in the azimuth, as in the experimental campaigns, even for a low mass flow, induces a localized increase in the neutral atom density that may play a role in the localized erosion profile. However, this effect cannot be observed in the simulations.

We can reasonably think that an increase in the mobility coefficient in the two-dimensional hybrid model in the case of magnetic field lines connecting the steering pole to the anode (namely, cases 2 and 4) would increase the discharge current without increasing the ion current, leading to a drop in the thruster anode efficiency (as observed in the experimental results). For simplicity, we have chosen a constant coefficient throughout the study to model the anomalous transport of the electrons across the radial magnetic field. Unfortunately, we are not able to quantify the influence of the magnetic field topology on the anomalous

transport of electrons. An additional source of difference between the experiments and calculations must certainly be attributed to the consequence of three-dimensional structure of the magnetic field on the axial electron mobility, especially if the azimuthal structure of the magnetic field is broken.

## VI. Conclusions

The effect of a modified magnetic field topography through an external magnetic steering structure, comprising four TSD pole pieces, and atom injection in the PPS®1350 was studied with a two-dimensional axisymmetric model. Although steering of the thrust vector is a three-dimensional problem, the two-dimensional model of the discharge is a useful tool that can be used to evaluate the proposed concept. The objectives were to analyze the capacities of such a system, to deviate the ion beam, and to study the resulting erosion of the ceramic walls. Different magnetic field configurations were tested varying the magnitude and the sign of the current passing through the external coils, with and without a supplementary injection of neutrals through the ceramic walls.

In some magnetic field configurations, the magnetic field lines passing through the cathode are directly connected to the anode plane. The electrons entering the channel are then rapidly collected by the anode, and the electron residence time in the channel is too short to efficiently ionize propellant, resulting in reduced thruster efficiency. A larger current passing through the coils causes a larger inclination of the magnetic field lines. The magnitude of the angle of deviation of the ion beam is directly linked to the magnitude of the currents in the TSD coils, because the magnetic field lines can be considered constant electric potential lines. The erosion of the ceramic walls is asymmetric and depends on the orientation of the ion beam, and the eroded thickness is related to the magnitude of the coil currents in the TSD structure.

To increase the ion beam deviation, a supplementary injection of neutrals has been tested (keeping constant the total mass flow of neutrals injected in the channel). Results show a low influence of only a few supplementary degrees, with an increase in wall erosion. The influence of a supplementary injection of neutrals is weak compared to the complexity of the system of neutral injection that must be used. As a result, the supplementary injection of neutrals as the sole method to deviate the ion beam is not justified.

The two-dimensional model results were used to define the initial conditions for a three-dimensional model of the plume to compare the calculated thrust vector with the measured value, because a complete three-dimensional model covering the channel and the plume region is not yet developed. Comparisons of experimental results with simulations investigated the effects a localized injection of neutral propellant and of the magnitude of the steering coil currents in the TSD structure. The study revealed the same trends, but differences have been observed. We can attribute theses discrepancies to three-dimensional effects such as the interactions between adjacent coils in the external structure and/or an injection of neutrals at a given azimuthal angle cannot be neglected and are not captured by the simplified approach in these simulations. Another source of differences can also be related to the poorly understood anomalous transport of the electrons across the magnetic field that has been considered as constant in this investigation. Therefore, the model is not able to reproduce all of the detailed results obtained in the experimental campaigns.

## Acknowledgments

The authors acknowledge support from the European Space Agency through the Technology Research Program no. 17159/03/NL/CH. The two-dimensional hybrid model has been developed in the framework of Groupement De Recherche Centre National de la Recherche Scientifique/Centre National dEtudes Spatiales/Société Nationale d'Étude et de Construction de Moteurs d'Aviation/Universités no. 3161 "Propulsion par Plasma dans l'Espace."

## References

[1] Leveque, N., Welch, C., Ellery, A., and Curley, A., "Trajectory Simulations for Thrust-Vectored Electric Propulsion Missions," International Electric Propulsion Conference Paper 03-050, 2003.

[2] Duchemin, O., Prioul, M., Illand, H., Banetta, S., Vicini, A., Garrigues, L., Rigollet, R., and Estublier, D., "Development of a Prototype Thrust Steering Device for Hall-Effect Thrusters," ESA SP 555, 2004.

[3] Biron, J., Cornu, N., Illand, H., Serrau, M., Rigollet, R., and Gray, H., "The Thruster Module Assembly (Hall-Effect Thruster) Design, Qualification and Flight," International Electric Propulsion Conference Paper 2005-213, 2005.

[4] Prioul, M., "Thrust Steering Devices Concepts Review for Hall-Effect Thrusters," ESA TRPTSD-SN-TN-0001, 2003.

[5] Day, M., Kim, V., Kozlov, V., Lazourenko, A., Popov, G., and Skrylnikov, A., "Investigation of the Possibility to Reduce Plume Divergence by Optimization of the Magnetic Field Topology in the Acceleration Channel," International Electric Propulsion Conference Paper 97-154, 1997.

[6] Lazurenko, A., Kim, V., Bishaev, A., and Auweter-Kurtz, M., "Three-Dimensional Simulation of Atom and Ion Dynamics in a Stationary Plasma Thruster," *Journal of Applied Physics*, Vol. 98, No. 4, 2005, p. 043303. doi:10.1063/1.2009821

[7] Duchemin, O., Illand, H., Saverdi, M., Cesari, U., Signori, M., Pagnon, D., and Estublier, D., "Testing of a Thrust Steering Device on the PPS®1350 Hall Thruster," AIAA Paper 2006-4478, 2006.

[8] Duchemin, O., Saverdi, M., and Estublier, D., "Performance and Lifetime Assessment of a Thrust Steering Device for PPS®1350 Hall-Effect Plasma Thruster," Paper No. 49, ESA SP-658, May 2008.

[9] Hagelaar, G. J. M., Bareilles, J., Garrigues, L., and Boeuf, J. P., "Two Dimensional Model of a Stationary Plasma Thruster," *Journal of Applied Physics*, Vol. 91, No. 9, 2002, p. 5592. doi:10.1063/1.1465125

[10] Garrigues, L., Hagelaar, G. J. M., Bareilles, J., Boniface, C., and Boeuf, P. J., "Model Study of the Influence of the Magnetic Field Configuration and a Performance and Lifetime of a Hall Thruster," *Physics of Plasmas*, Vol. 10, No. 12, 2003, p. 4886. doi:10.1063/1.1622670

[11] Bareilles, J., "Modélisation 2D Hybride d'un Propulseur à Effet Hall pour Satellite," Ph.D. Thesis Univ. Paul Sabatier, Toulouse, France, 2002 (in French).

[12] Boniface, C., "Modélisation et Diagnostics d'un Propulseur Effet Hall pour Satellites: Configuration Magnétique et Nouveaux Concepts," Ph.D. Thesis Univ. Paul Sabatier, Toulouse, France, 2006 (in French).

[13] Garrigues, L., Hagelaar, G. J. M., Boniface, C., and Boeuf, P. J., "Optimized Atom Injection in a Hall-Effect Thruster," *Applied Physics Letters*, Vol. 85, No. 22, 2004, p. 5460. doi:10.1063/1.1829137

[14] Boniface, C., Garrigues, L., Hagelaar, G. J. M., Boeuf, J. P., Gawron, D., and Mazouffre, S., "Anomalous Cross Field Electron Transport in a Hall Effect Thruster," *Applied Physics Letters*, Vol. 89, No. 16, 2006, p. 161503. doi:10.1063/1.2360182

[15] Bareilles, J., Hagelaar, G. J. M., Garrigues, L., Boniface, C., Boeuf, J. P., and Gascon, N., "Critical Assessment of a Two Dimensional Hybrid Hall Thruster Model: Comparisons with Experiments," *Physics of Plasmas*, Vol. 11, No. 6, 2004, p. 3035. doi:10.1063/1.1719022

[16] Kim, V., "Main Physical Features and Processes Determining the Performance of Stationary Plasma Thrusters," *Journal of Propulsion and Power*, Vol. 14, No. 5, 1998, p. 736. doi:10.2514/2.5335

[17] Sommier, E., Scharfe, M. K., Gascon, N., Capelli, M. A., and Fernandez, E., "Simulating Plasma Induced Hall Thruster Wall Erosion with a Two-dimensional Hybrid Model," *IEEE Transactions on Plasma Science*, Vol. 35, No. 5, 2007, p. 1379. doi:10.1109/TPS.2007.905943

[18] Garrigues, L., Hagelaar, G. J. M., Boniface, C., and Boeuf, J. P., "Anomalous Conductivity and Secondary Electron Emission in Hall Effect thrusters," *Journal of Applied Physics*, Vol. 100, No. 12, 2006, p. 123301. doi:10.1063/1.2401773

[19] Yamamura, Y., and Tawara, H., "Energy Dependence of Ion-Induced Sputtering Yields from Monatomic Solids at Normal Incidence," *Atomic Data and Nuclear Data Tables*, Vol. 62, No. 2, 1996, p. 149. doi:10.1006/adnd.1996.0005; Erratum in *Atomic Data and Nuclear Data Tables*, Vol. 63, No. 2, 1996, p. 353. doi:10.1006/adnd.1996.0016

[20] Garnier, Y., Viel, V., Roussel, J. F., and Bernard, J., "Low-Energy Xenon Ion Sputtering of Ceramics Investigated for Stationary Plasma Thrusters," *Journal of Vacuum Science and Technology A: Vacuum, Surfaces, and Films*, Vol. 17, No. 6, 1999, p. 3246. doi:10.1116/1.582050

[21] Passaro, A., Vicini, A., and Biagioni, L., "3D Computation of Thruster Plasma Plumes," AIAA Paper 2004-3632, 2004.

[22] Pagnon, D., Touzeau, M., and Lasgorceix, P., "Control of the Ceramic Erosion by Optical Emission Spectroscopy: Parametric Studies of SPT100-ML," AIAA Paper 04-3773, 2004.

A. Gallimore
*Associate Editor*